Theor Chem Acc (2016) 135:9
DOI 10.1007/s00214-015-1766-8

REGULAR ARTICLE

Thermolysis biradical mechanisms in endoperoxides: A challenge for density functional theory?

Martial Boggio-Pasqua[1] · **Jean-Louis Heully**[1]

Received: 28 September 2015 / Accepted: 16 November 2015 / Published online: 22 December 2015

Abstract We report a theoretical study of the thermal decomposition of benzene endoperoxide. A comparison between unrestricted density functional theory (UDFT) and highly correlated multireference ab initio methods has been carried out in order to assess the accuracy and reliability of UDFT to describe biradical mechanisms. The conclusion is that UDFT is a promising tool to describe the biradical mechanisms of endoperoxides. However, it can fail in the particular case of high multiconfigurational character associated with a rather weak biradical character, which happens in the first step of the stepwise cycloreversion mechanism of the prototype system studied, depending on the exchange–correlation functional used. Thus, caution has to be taken when arguing about the possible non-existence of biradical pathways with UDFT.

Keywords Endoperoxide · Cycloreversion · Homolysis · Broken-symmetry density functional theory · Ab initio calculations · Biradical mechanism

1 Introduction

Endoperoxides (EPOs) belong to a family of compounds able to release singlet oxygen $^1O_2$ under heating or UV irradiation, an exceptional feature which makes these compounds highly interesting for various applications. In particular, highly reactive $^1O_2$ and other reactive oxygen species play a key role in biological and biochemical processes [1]. They are also critical in photodynamic therapy due to their extraordinary high oxidation potential [2]. This property can be exploited for selective destruction of cancer cells and skin diseases, for example [3, 4]. Thus, understanding the thermolysis and photolysis of EPOs is of prime importance to benefit from the formidable potential of these versatile compounds.

Two primary pathways of transformation may compete during thermolysis or photolysis of aromatic EPOs (Scheme 1): (1) cycloreversion, leading to the parent aromatic hydrocarbon and to singlet or triplet oxygen, and (2) homolytic cleavage of the peroxidic bond, which can be followed by rearrangement to diepoxides (not represented in Scheme 1) or by decomposition to hydroxyketones or quinones. The branching ratio between these two competing processes depends on the EPO chemical structure and on experimental conditions [5].

The photochemistry of EPOs has been investigated in detail both theoretically [6–14] and experimentally [15–22]. One of the main conclusions is that the two main photolysis pathways depend on the nature of the excited electronic state that is populated: While $\pi\pi^*$ states are responsible for cycloreversion, $\pi\sigma^*$ states can lead to homolytic cleavage of the peroxidic bond. While the thermal decomposition of EPOs is well characterized from an experimental standpoint [23–25], relatively few theoretical studies [26] have been reported on the two competing thermolysis pathways. However, a number of theoretical studies have been devoted to the addition of singlet oxygen to benzene and longer acenes [26–29]. One of the main difficulties in studying theoretically the competition between these two thermal decomposition processes

Electronic supplementary material The online version of this article (doi:10.1007/s00214-015-1766-8) contains supplementary material, which is available to authorized users.

✉ Martial Boggio-Pasqua
martial.boggio@irsamc.ups-tlse.fr

[1] Laboratoire de Chimie et Physique Quantiques (UMR 5626), CNRS et Université de Toulouse 3, Toulouse, France

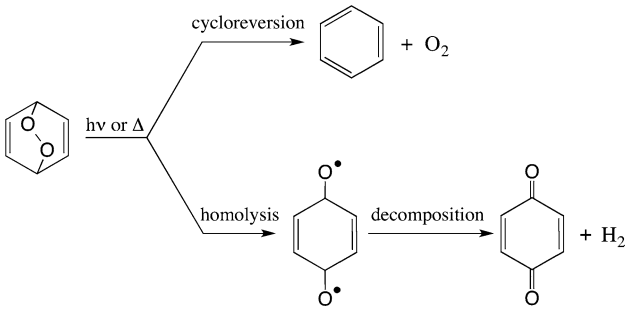

Scheme 1 Possible transformation of CHDEPO during thermolysis or photolysis

is that several biradical intermediates are involved along the reaction paths. While multiconfigurational ab initio calculations, such as the complete active space self-consistent field (CASSCF) method and its extension to second-order perturbation theory (CASPT2), can be used reliably to describe these biradical pathways, they become rapidly too expensive when the size of the system becomes too large. These methods can be used routinely for studying the thermolysis and photolysis of benzene EPO (also called cyclohexadiene EPO and denoted CHDEPO in the following) but are unworkable for longer acenes (naphthalene and beyond) unless further approximations are made to reduce the number of configurations generated [30–34] or to treat very large active spaces [35–38]. Thus, there is an incentive to use less demanding methods based on density functional theory (DFT) since many biradical species are too large to be treated with correlated multireference ab initio methods. Broken-symmetry unrestricted DFT (BS-UDFT) calculations using a spin-projected correction scheme [39–41] for the energies have proved reliable to describe singlet biradical mechanisms provided appropriate functionals are used [42]. In particular, it has been used by Bendikov et al. [26] to study the Diels–Alder reaction of acenes (benzene through pentacene) with molecular oxygen. However, no comparison was made with accurate ab initio calculations to verify the validity of their UDFT results. Here, we report a theoretical study of the thermolysis mechanisms of CHDEPO based on the comparison of accurate multiconfigurational ab initio calculations and UDFT calculations. This study brings some insight into the two competing thermal decomposition pathways of this species, as shown in Scheme 1, and illustrates the limitations of using an unrestricted DFT formalism in this particular case. It also shows that one has to be careful when drawing mechanistic conclusions from UDFT calculations on biradical mechanisms.

2 Computational details

Restricted DFT and unrestricted DFT calculations were performed for all closed-shell and open-shell species, respectively. For open-shell species, permuted orbitals (PO) and BS-UDFT calculations were performed. These calculations result from different constructions of initial guesses, as explained in references [43, 44]. Spin-projected energies have been calculated with the approximate spin-correction procedure proposed by Yamaguchi and coworkers [39, 40] (Table S1 in Electronic Supplementary Material). The M06-2X functional [45] was used throughout, as it has been tested and recommended to treat open-shell singlet biradicals [42]. The 6-311G** basis set was used on all atoms. The structures of all the critical points have been fully optimized (Tables S2–S10 in Electronic Supplementary Material) using an analytical gradient procedure with the methods available in the Gaussian 09 package of programs [46]. Harmonic frequency analyses were performed in order to determine the nature (minimum or transition state) of the critical points found. Natural orbitals (Table S11 in Electronic Supplementary Material) and spin densities (Table S12 in Electronic Supplementary Material) were computed to evaluate the biradical character of the optimized species.

Geometry optimizations were also performed at the CASSCF level of theory (Tables S13–S22 in Electronic Supplementary Material) using a 6-31G* basis set. Unless otherwise specified, the active space used throughout the calculations includes the complete π valence space (two pairs of π_{CC}/π^*_{CC} and π_{OO}/π^*_{OO}) and the σ orbitals involving the two oxygen atoms $\sigma_{CO}/\sigma^*_{CO}$ (two pairs) and $\sigma_{OO}/\sigma^*_{OO}$, necessary to properly account for O–O homolysis and cycloreversion. This comprises altogether a total of 14 electrons distributed into 12 orbitals, denoted CASSCF (14,12) in the following. The orbitals are provided as supplementary material for CHDEPO (Figure S1 in Electronic Supplementary Material). State-averaged (SA) calculations over at least two states (ground and first singlet excited states) were necessary in order to preserve the active space along the homolysis and cycloreversion pathways considered in this study. Final energies were calculated at these CASSCF optimized geometries using the internally contracted CASPT2 method [47] along with the correlation-consistent triple-ζ (cc-pVTZ) basis set. We also used the CIPT2 method [48], which is a coupling between multireference configuration interaction and multireference perturbation theory. To estimate the importance of higher-order correlations, a Davidson correction (denoted CIPT2 + Q) was applied. A level shift of 0.2 Hartree was adopted to avoid intruder state problems in both the CASPT2 and CIPT2 calculations. All these multireference calculations

have been performed with the MOLPRO quantum chemistry package [49]. Note that we did not include any corrections for the basis set superposition error (BSSE), as the purpose of this work is to compare the DFT and ab initio mechanistic pictures rather than to obtain the most accurate energies for the thermolysis of this prototype EPO.

Electronic structures have been determined exploiting the results of the computation of the spin-exchange density matrix P_{ij} and the diagonal elements of the one-electron density matrix at the CASSCF level (see Ref. [50] for details). The elements of P_{ij} have a simple physical interpretation, which is related to the spin coupling between the electrons localized in the orbitals residing on the atoms i and j [51]. An illustration of the meaning of these matrix elements can be found in Ref. [50]. The code to calculate the CASSCF P_{ij} matrix is implemented in Gaussian 09. We also analyzed the CASSCF natural orbital occupation numbers (NOONs), i.e., the eigenvalues of the ground-state density matrix (Table S23 in Electronic Supplementary Material). Here, the eigenvalues close to one (or significantly different from zero or two) reflect the biradical character of the wavefunction. Direct comparison can then be made with the NOONs found at the UDFT level in order to compare the biradical characters found at the two levels of theory.

3 Results and discussion

3.1 Cycloreversion mechanism

Two possible mechanisms have been identified for the cycloreversion pathway. Energies and bond distances are given at the CIPT2 and CASSCF levels, respectively, unless otherwise specified. As shown in Fig. 1, the lowest energy path involves a concerted mechanism in which the transition state (TS_{Conc}) displays two equally elongated CO bonds (1.9 Å, Fig. 2). The energy barrier of this synchronous activated process amounts to 0.86 eV, and the benzene and singlet oxygen products (M_{B+O_2}) generated are slightly lower in energy (by 0.12 eV) than the original EPO reactant (M_{CHDEPO}). These results are in good agreement with a previous CASSCF study including quasi-degenerate perturbation theory (MCQDPT2) providing a barrier of 0.92 eV and locating the product 0.16 eV below the EPO reactant [29]. The analysis of the CASSCF electronic structure at TS_{Conc} shows a weak biradical character on both the benzene and oxygen moieties, as the NOON closest to one is only 0.17 (Fig. 3; Table S23).

The second mechanism involves a stepwise process in which the two CO bonds are broken sequentially. In a first step, one CO bond is broken (3.9 Å), leading to a biradical intermediate denoted M_{int} lying 0.94 eV above the

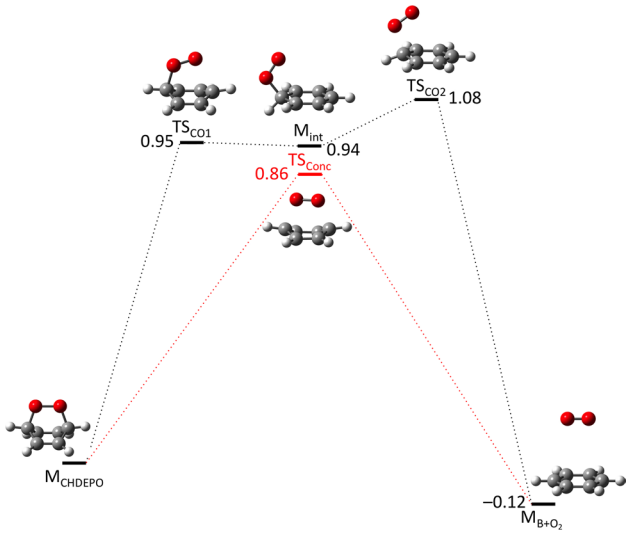

Fig. 1 CIPT2 energies (eV) for biradical stepwise (*black*) and concerted (*red*) cycloreversion pathways relative to CHDEPO. The minimum energy (M) and transition-state (TS) structures obtained at the CASSCF level are also shown

reactant. The transition state involved in this step (TS_{CO_1}) lies close in energy to the M_{int} intermediate and displays a rather weak biradical character with a NOON of only 0.34 (Fig. 3; Table S23), as a result of the CO bond being broken (2.2 Å, Fig. 2). At M_{int}, the biradical character is already very strong (two NOONs close to one). In the second step, the other CO bond is being elongated (1.8 Å at TS_{CO_2}) with an energy barrier of 0.14 eV. At this transition state, both the benzene and singlet oxygen moieties acquire a biradical character (Fig. 3; Table S23). These results are consistent with previous multistate (MS)-CASPT2 results [6] in which the second step of the stepwise mechanism was characterized (see Table 1). Note that Bobrowski et al. failed to determine this asynchronous mechanism in their CASSCF/MCQDPT2 study [29]. Table 1 shows that CASPT2 results with a larger basis set and inclusion of Davidson corrections at the CIPT2 level (CIPT2 + Q) do not affect significantly the results.

The results of the UDFT calculations are reported in Table 1 for energies and in Fig. 2 for structures. The concerted path is fairly well reproduced by the UDFT calculations in terms of both energies and geometrical structures. The barrier at TS_{Conc} is 1.12 eV, in good agreement with the 1.19 eV energy barrier found by Bendikov et al. [26]. The main structural deviation with the CASSCF geometries concerns the OO bond length that is significantly shorter at the DFT level (by 0.05 at M_{B+O_2} up to 0.1 Å at M_{CHDEPO}). Note that from crystal structures of 1,4-peroxides formed from aromatic compounds, the OO bond length is determined to be between 1.47 [52, 53] and 1.50 Å [54] at intermediate values between the CASSCF and M06-2X bond lengths.

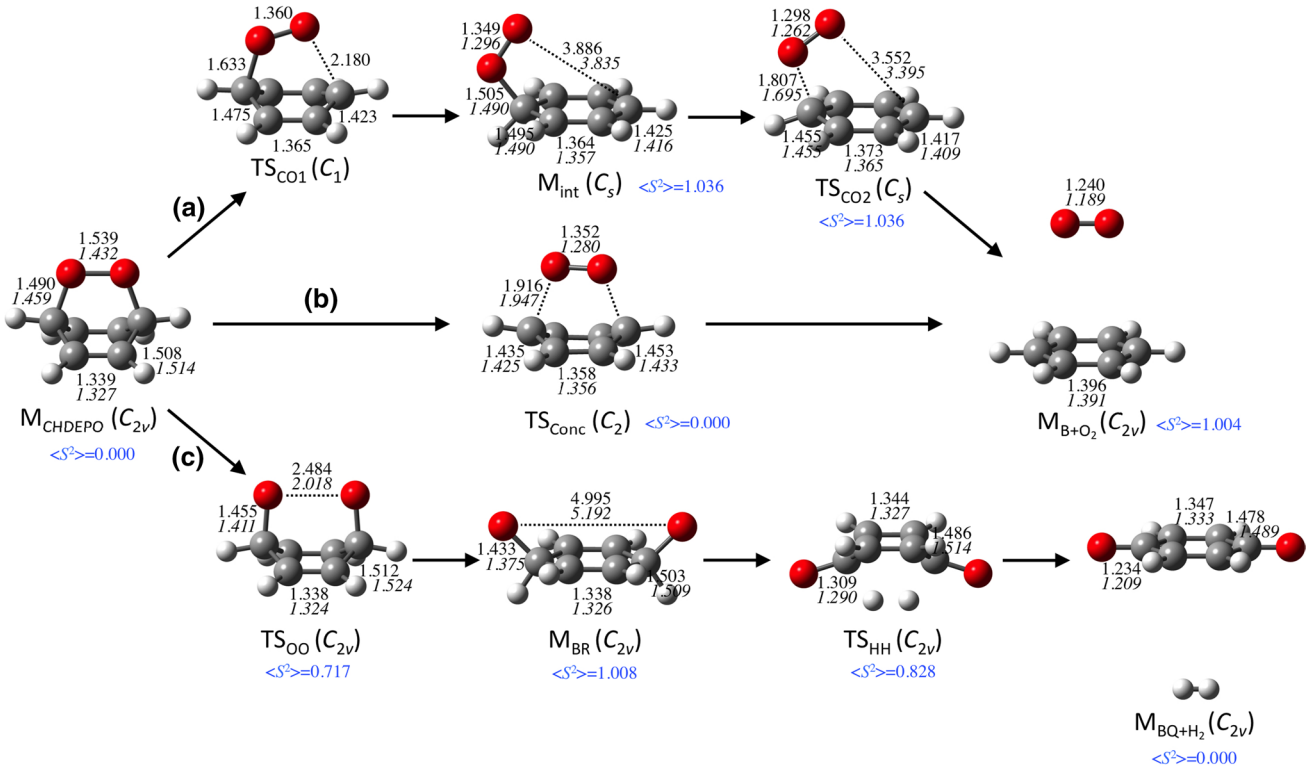

Fig. 2 Geometrical structures along (**a**) the biradical stepwise and **(b)** the concerted cycloreversion pathways, and along (**c**) the biradical O–O homolysis and decomposition to benzoquinone pathway. All distances are in Å. CASSCF values in normal font and DFT values in italics. $\langle S^2 \rangle$ expectation values obtained with DFT are indicated. The symmetry point group for each structure is indicated in parentheses

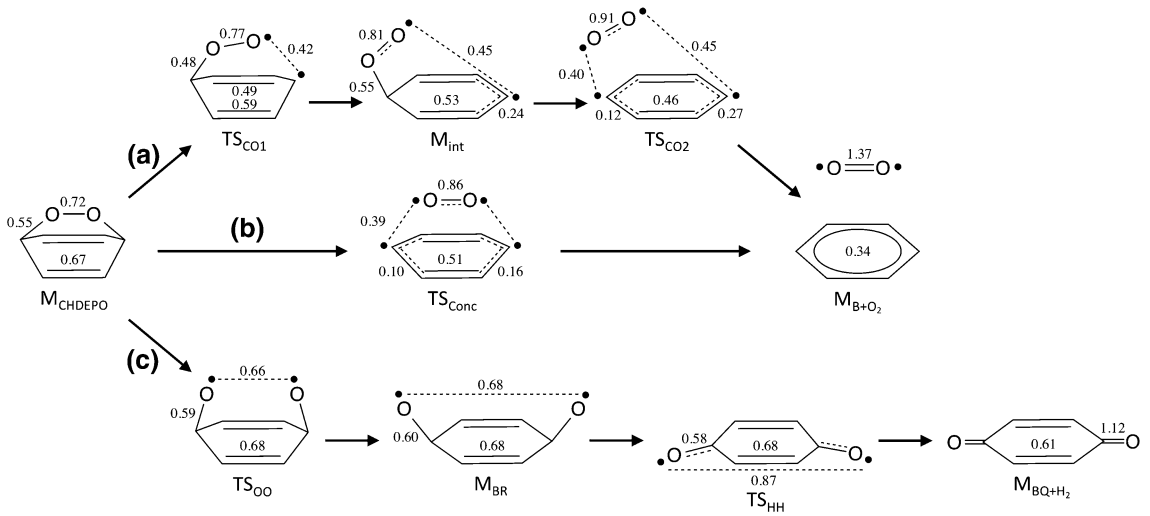

Fig. 3 Electronic structures and values of the spin-exchange density matrix along **(a)** the biradical stepwise and **(b)** the concerted cycloreversion pathways, and along **(c)** the biradical O–O homolysis and decomposition to benzoquinone pathway

Regarding the change in electronic structure along this path, the CASSCF wavefunction shows a weak biradical character of both the benzene and oxygen moieties at TS_{Conc}, as discussed above. The CASSCF wavefunction is dominated by a closed-shell determinant (78 %) followed by several biexcited configurations with much smaller weights (ca. 1 %). Not surprisingly, the UDFT self-consistent field (SCF) solution collapses to the closed-shell singlet determinant dominating the CASSCF wavefunction and thus does not describe the weak open-shell character of this transition

Table 1 Energies (eV) for biradical and concerted cycloreversion pathways relative to CHDEPO at different levels of theory

Structure	UM06-2X/6-311G**	MS-CASPT2/ANO	SA2-CASSCF/6-31G*	CASPT2/VTZ	CASPT2/VQZ	CIPT2/VTZ	CIPT2 + Q/VTZ
M_{CHDEPO}	0	0	0	0	0	0	0
TS_{CO_1}	n.f.	n.a.	0.987	0.833	0.835	0.950	0.920
M_{int}	0.974	0.90[a]	0.504	0.873	0.897	0.943	0.970
TS_{CO_2}	1.222	1.20[a]	0.782	0.872	0.891	1.080	1.081
M_{B+O_2}	0.117	0.01[a]	−1.012	−0.280	−0.252	−0.122	−0.040
TS_{Conc}	1.124	n.a.	0.970	0.726	0.723	0.856	0.813

n.f. not found, *n.a.* not available

[a] Ref. [6]

state. However, it gives reliable information on the energy and geometrical structure of this species, as the main configuration is a closed-shell determinant. For the benzene plus oxygen product, the DFT SCF solution is converging to the singlet closed-shell benzene and the singlet biradical state of O_2 (Tables S11 and S12 in Electronic Supplementary Material). Thus, a reliable description of the potential energy profile along the concerted pathway is obtained with UDFT, in agreement with CASSCF/CASPT2.

The case of the stepwise mechanism proved to be quite different. It was not possible to locate the TS_{CO_1} transition state at the unrestricted M06-2X level. All attempts to optimize this structure ended up collapsing to the closed-shell SCF solution of the concerted path (i.e., TS_{Conc}). This result is consistent with previous theoretical studies [26–29], which concluded that the concerted path was the preferred one for the reaction of benzene with singlet oxygen. However, we would like to point out that because a singlet biradical pathway is not found with BS-UDFT does not mean it cannot exist. The existence of the minima M_{CHDEPO} and M_{int} means that there is necessarily a transition state connecting these two structures. The CASSCF wavefunction at TS_{CO_1} shows a strong multiconfigurational character and a weak biradical character. The major configuration corresponds to a closed-shell determinant with a weight of only 66 %. Many other determinants involving mono- and biexcited configurations play an important role, and some of these are responsible for the rather weak biradical character of the wavefunction. With M06-2X, the SCF solution collapses immediately to the closed-shell determinant leading, upon optimization, to the synchronous transition state. It is worth noting that the multiconfigurational character at TS_{CO_1} is not surprising, as this transition state connects two minima corresponding to two completely different electronic states. In other words, this transition state results from an avoided crossing that sits on the "shoulder" of a conical intersection between the ground state and an excited state (see Figure 3 in Ref. [6]). As a result, the electronic structure is heavily mixed in that region of the potential energy surface.

While it is true that DFT is a monodeterminantal method, which thus cannot pick up all these configurations, it is an exact theory which, in principle, could determine exactly the electron density of a system and thus its energy if the exact exchange–correlation functional was known. In DFT, the mixing of electronic configurations occurs through the electron density instead of the electron configurations in a multiconfigurational wavefunction-based method such as CASSCF. Examples of multiconfigurational transition states optimized with unrestricted DFT can be found in references [55–59]. Here we tested all the various hybrid functionals and long-range corrected functionals available in Gaussian 09 to assess their performance in finding TS_{CO_1}. Several scenarios can be distinguished. In the first one, which was the most frequently encountered, the SCF solution collapses immediately to the closed-shell determinant. This was the case in most of the functionals tested (including the popular B3LYP [60], PBE0 [61], M06 [45], TPSSh [62], HSE06 [63] and ωB97X-D [64]). In such cases, the transition-state search inevitably ends up finding TS_{Conc}. In the second scenario, a few functionals (e.g., MPWB1K [65], CAM-B3LYP [66] and ωB97 [67]) allow finding the BS solution, but optimization of the transition state leads to TS_{Conc} because no stationary point corresponding to TS_{CO_1} exists. Finally, the third scenario, which was encountered with half-and-half functionals [68] (BHandH and BHandHLYP) and with LC-ωPBE [69], is that not only the BS solution is stable, but also a stationary point corresponding to TS_{CO_1} could be found. With BHandH and BHandHLYP, the stationary point is characterized by one imaginary frequency corresponding to the CO stretching of the breaking CO bond, as expected. However, with LC-ωPBE, two imaginary frequencies were found. The largest one corresponds to the stretching of the breaking CO bond, and the lower one corresponds to the stretching of the other CO bond. Thus, LC-ωPBE represents a case at the limit between the second and third scenarios, as the stationary point located is unstable against stretching of the second CO bond, thus producing a second-order saddle point. It is also

interesting to note that by increasing progressively the percentage of exact Hartree–Fock exchange (E_{xc}^{HF}) in B3LYP, the situation evolves from scenario 1 (E_{xc}^{HF} < ~30 %) to scenario 2 (~30 % ≤ E_{xc}^{HF} < ~40 %) and then to scenario 3 (E_{xc}^{HF} ≥ ~40 %). With BHandH and BHandHLYP, the energy barrier for the first step is calculated at 1.296 and 1.085 eV, respectively, while LC-ωPBE gives an intermediate value of 1.244 eV. M_{int} is located 0.35 and 0.66 eV below TS_{CO_1} with the two half-and-half functionals, respectively, and 0.43 eV below with LC-ωPBE. These results are in good agreement with the CASSCF value of 0.48 eV. It is likely that TS_{CO_1} is too low in energy at the CIPT2 level due to the approximate CASSCF structure used, as the position of a transition state is sensitive to the energy difference between the two minima it interconnects (cf. Hammond's postulate [70]). At the CASSCF level, the energy difference between M_{CHDEPO} and M_{int} is only 0.5 eV, whereas it is nearly double this value at the CIPT2 and M06-2X levels. Thus, one can expect that TS_{CO_1} should lie closer to the M_{int} structure than it does at the CASSCF level. Note also that BS optimized geometries at the UDFT level suffer from the spin contamination [71, 72] and are therefore less reliable than optimized geometries of closed-shell singlet species.

In addition, UDFT describes accurately the second step of the stepwise mechanism. The intermediate M_{int} is located 0.97 eV above M_{CHDEPO}, and the energy barrier for this second step is calculated at 0.25 eV, in good agreement with the CIPT2 results. The biradical character at M_{int} and TS_{CO_2} are correctly described (Tables S11 and S12 in Electronic Supplementary Material), giving a pair of nearly singly occupied natural orbitals similar to the CASSCF one for each structure (compare Tables S11 and S23 in Electronic Supplementary Material).

3.2 Mechanism of peroxidic bond homolysis and decomposition to benzoquinone

The pathway for the O–O homolysis mechanism leading to the benzoquinone product has been characterized. As shown in Fig. 4, this path involves a stepwise mechanism in which the OO bond and two CH bonds are broken sequentially. In a first step, the OO bond is broken (5.0 Å, Fig. 2), leading to a biradical intermediate denoted M_{BR} lying 0.83 eV above the reactant (Fig. 4; Table 2). The transition state involved in this step (TS_{OO}) lies 1.25 eV above the reactant M_{CHDEPO} and displays a substantial biradical character (Fig. 3; Table S23 in Electronic Supplementary Material), as a result of the OO bond being broken (2.5 Å, Fig. 2). In the second step, two CH bonds are being elongated synchronously (1.4 Å at TS_{HH}) with an energy barrier of 0.31 eV. At this transition state, the biradical character is still substantial (Fig. 3; Table S23 in Electronic Supplementary Material). Finally, the benzoquinone and molecular hydrogen products (M_{BQ+H_2}) are located 2.8 eV below the EPO reactant. These results are in good agreement with previous MS-CASPT2 results [6, 10], except for the TS_{HH} transition state which was located 0.38 eV higher in energy at this level of calculation.

The results of the UDFT calculations (Table 2; Fig. 2c) are consistent with this mechanism. The OO homolysis involves a barrier at TS_{OO} of 0.97 eV, 0.28 eV lower than the CIPT2 result but 0.12 eV higher than the MS-CASPT2 result. At this transition state, the OO bond length has increased by 0.59 Å (0.95 Å at CASSCF level). The M_{BR} intermediate is located 0.62 eV above M_{CHDEPO}, i.e., 0.2 eV lower than the corresponding CIPT2 value. The structure of M_{BR} is in good agreement with the CASSCF one, except maybe for the CO bond lengths which are 0.06 Å shorter at the M06-2X level. The step for decomposition

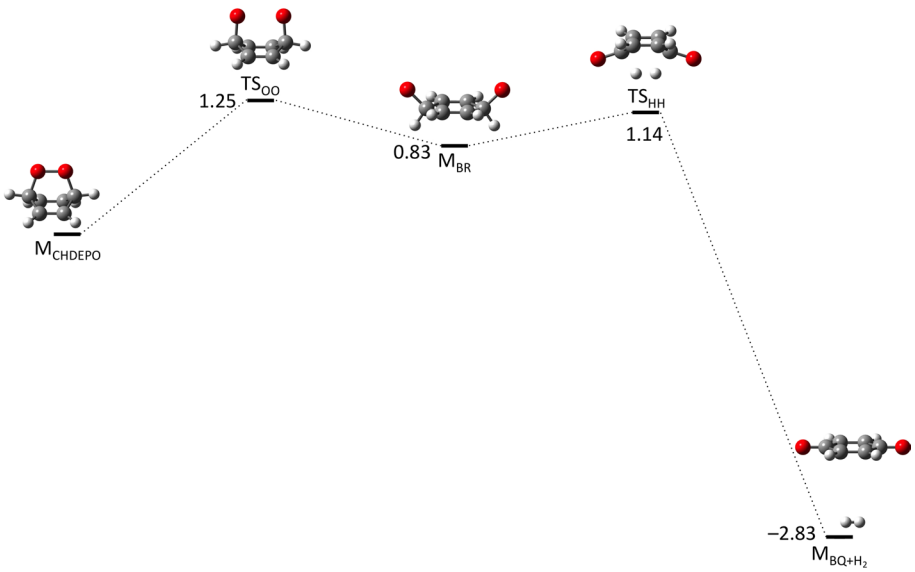

Fig. 4 CIPT2 energies (eV) for biradical O–O homolysis and decomposition to benzoquinone pathway relative to CHDEPO. The minimum energy (M) and transition-state (TS) structures obtained at the CASSCF level are also shown

Table 2 Energies (eV) for biradical O–O homolysis and decomposition to benzoquinone pathway relative to CHDEPO at different levels of theory

Structure	UM06-2X/6-311G**	MS-CASPT2/ANO	SA2-CASSCF/6-31G*	CASPT2/VTZ	CASPT2/VQZ	CIPT2/VTZ	CIPT2 + Q/VTZ
M_{CHDEPO}	0	0	0	0	0	0	0
TS_{OO}	0.971	0.85[a]	0.712	1.291	1.316	1.253	1.315
M_{BR}	0.624	0.52,[a] 0.85[b]	0.207	0.907	0.936	0.829	0.906
TS_{HH}	1.456	1.52[b]	3.075	1.049	1.035	1.141	1.158
M_{BQ+H_2}	−2.724	−2.77[b]	−3.678[c]	−2.812, −2.644[c]	−2.825	−2.834, −2.779[c]	−2.820, −2.715[c]

[a] Ref. [10]

[b] Ref. [6]

[c] Computed with a (16e, 14o) active space

to benzoquinone involves a barrier of 0.83 eV at TS_{HH}, in good agreement with the MS-CASPT2 value of 0.67 eV, but substantially higher than the CIPT2 value of 0.31 eV. At this transition state, the CH bonds have been synchronously stretched by 0.19 Å (0.32 Å at CASSCF level). Finally, the M_{BQ+H_2} products are located 2.72 eV below M_{CHDEPO}, in very good agreement with MS-CASPT2 and CIPT2 results. In addition, the UDFT method describes correctly the biradical character of these two steps: The M_{BR} biradical intermediate is characterized by a pair of nearly singly occupied natural orbitals, while in the two transition states TS_{OO} and TS_{HH}, only about half of an electron has been transferred, in agreement with CASSCF (compare Tables S11 and S23 in Electronic Supplementary Material).

4 Conclusions

We report in this study a theoretical study of the thermal decomposition of benzene (or cyclohexadiene) EPO. The small size of this prototype system allows accurate benchmark calculations to be performed based on multireference ab initio calculations (CASPT2, CIPT2) against which DFT calculations can be compared. Due to the intrinsic biradical character of the two decomposition pathways investigated (i.e., cycloreversion and OO homolysis followed by decomposition to benzoquinone), BS and PO DFT calculations have been performed. This study shows that some accurate information on the potential energy profiles (applying a spin-projected correction scheme), structural changes and electronic structure reorganizations along these biradical mechanisms can be obtained from the UDFT calculations. However, in this particular case, the information is incomplete at the M06-2X level, as one important transition state could not be found. While two possible mechanisms, concerted and stepwise, have been identified for the cycloreversion with highly correlated ab initio methods, BS M06-2X calculations fail to locate the first transition state (TS_{CO_1}) of the stepwise mechanism. Rather, the transition-state optimization collapses to the transition state of the concerted pathway (TS_{Conc}). At TS_{CO_1}, the CASSCF wavefunction is highly multiconfigurational and the biradical character is rather weak making the case difficult for BS-UDFT. The test of various density functionals produced different behaviors. While most functionals failed to find a stable BS solution in that region of the potential energy surface, a few functionals, however, allowed finding TS_{CO_1}. This is the case with half-and-half functionals and modified B3LYP functionals with an increased admixture of exact Hartree–Fock exchange.

To summarize, UDFT in the form of PO and BS-DFT is certainly a promising tool to investigate biradical mechanisms of larger EPOs and other biradical species. Yet, the potential multiconfigurational and weak biradical character of some intermediate structures should be a concern when using such an approach, as UDFT may fail to locate the associated biradical pathway. As a consequence, carefulness should to be taken before claiming about the possible non-existence of biradical pathways based solely on UDFT calculations.

Acknowledgments This work was granted access to the HPC resources of CALMIP under the allocation 2015-[12158].

References

1. Choea E, Min DB (2006) Crit Rev Food Sci Nutr 46:1–22
2. Henderson BW, Dougherty T (1992) Photochem Photobiol 55:145–157
3. DeRosa MC, Crutchley RJ (2002) Coord Chem Rev 233(234):351–357
4. Foote CS (1984) Mechanisms of photooxidation. In: Doiron DG, Gomer CJ (eds) Porphyrin localization and treatment of tumors. Alan R. Liss, Inc., New York, pp 3–18
5. Aubry JM, Pierlot C, Rigaudy J, Schmidt R (2003) Acc Chem Res 36:668–675
6. Martinez-Fernandez L, González L, Corral I (2015) J Chem Theory Comput 11:406–414
7. Kupfer S, Pérez-Hernández G, González L (2012) Theor Chem Acc 131:1295

8. Martinez-Fernandez L, González L, Corral I (2011) Comput Theor Chem 975:13–19
9. Mollenhauer D, Corral I, González L (2010) J Phys Chem Lett 1:1036–1040
10. Corral I, González L (2010) Chem Phys Lett 499:21–25
11. Corral I, González L (2008) J Comput Chem 29:1982–1991
12. Corral I, González L (2007) Chem Phys Lett 446:262–267
13. Kearns DR, Khan AU (1969) Photochem Photobiol 10:193–210
14. Kearns DR (1969) J Am Chem Soc 91:6554–6563
15. Corral I, González L, Lauer A, Freyer W, Fidder H, Heyne K (2008) Chem Phys Lett 452:67–71
16. Fidder H, Lauer A, Freyer W, Koeppe B, Heyne K (2009) J Phys Chem A 113:6289–6296
17. Lauer A, Dobryakov AL, Kovalenko SA, Fidder H, Heyne K (2011) Phys Chem Chem Phys 18:8723–8732
18. Klein A, Kalb M, Gudipati MS (1999) J Phys Chem A 103:3843–3853
19. Eisenthal KB, Turro NJ, Dupuy CG, Hrovat DA, Langan J, Jenny TA, Sitzmann EV (1986) J Phys Chem 90:5168–5173
20. Schmidt R, Schaffner K, Trost W, Brauer HD (1984) J Phys Chem 88:956–958
21. Gudipati MS, Klein A (2000) J Phys Chem A 104:166–167
22. Brauer HD, Schmidt R (2000) J Phys Chem A 104:164–165
23. Günther SG, Lemp EM, Zanocco AL (2002) J Photochem Photobiol A Chem 151:1–5
24. Twarowski AJ, Good L, Busch G (1988) J Phys Chem 92:396–402
25. Turro NJ, Chow MF, Rigaudy J (1981) J Am Chem Soc 103:7218–7224
26. Reddy AR, Bendikov M (2006) Chem Commun 1179–1181
27. Chien SH, Cheng MF, Lau KC, Li WK (2005) J Phys Chem A 109:7509–7518
28. Leach AG, Houk KN (2002) Chem Commun 1243–1255
29. Bobrowski M, Liwo A, Oldziej S, Jeziorek D, Ossowski T (2000) J Am Chem Soc 122:8112–8119
30. Boggio-Pasqua M, Groenhof G (2014) Comput Theor Chem 1040–1041:6–13
31. Krausbeck F, Mendive-Tapia D, Thom AJW, Bearpark MJ (2014) Comput Theor Chem 1040–1041:14–19
32. Sauri V, Serrano-Andrés L, Shahi ARM, Gagliardi L, Vancoillie S, Pierloot K (2011) J Chem Theory Comput 7:153–168
33. Ma D, Manni GL, Gagliardi L (2011) J Chem Phys 135:044128
34. Manni GL, Ma D, Aquilante F, Olsen J, Gagliardi L (2013) J Chem Theory Comput 9:3375–3384
35. Yanai T, Kurashige Y, Neuscamman E, Chan GKL (2010) J Chem Phys 132:024105
36. Shepard R, Gidofalvi G, Brozell SR (2014) J Chem Phys 141:064105
37. Aquilante F, Malmqvist PÅ, Pedersen TB, Ghosh A, Roos BO (2008) J Chem Theory Comput 4:694–702
38. Györffy W, Shiozaki T, Knizia G, Werner HJ (2013) J Chem Phys 138:104104
39. Yamaguchi K, Jensen F, Dorigo A, Houk KN (1988) Chem Phys Lett 149:537–542
40. Yamanaka S, Kawakami T, Nagao H, Yamaguchi K (1994) Chem Phys Lett 231:25–33
41. Ovchinnikov AA, Labanowski JK (1996) Phys Rev A 53:3946–3952
42. Ess DH, Cook TC (2012) J Phys Chem A 116:4922–4929
43. Cremer D (2001) Mol Phys 99:1899–1940
44. Gräfenstein J, Kraka E, Filatov M, Cremer D (2002) Int J Mol Sci 3:360–394
45. Zhao Y, Truhlar DG (2008) Theor Chem Acc 120:215–241
46. Frisch MJ, Trucks GW, Schlegel HB, Scuseria GE, Robb MA, Cheeseman JR, Scalmani G, Barone V, Mennucci B, Petersson GA, Nakatsuji H, Caricato M, Li X, Hratchian HP, Izmaylov AF, Bloino J, Zheng G, Sonnenberg JL, Hada M, Ehara M, Toyota K, Fukuda R, Hasegawa J, Ishida M, Nakajima T, Honda Y, Kitao O, Nakai H, Vreven T, Montgomery JA Jr, Peralta JE, Ogliaro F, Bearpark M, Heyd JJ, Brothers E, Kudin KN, Staroverov VN, Kobayashi R, Normand J, Raghavachari K, Rendell A, Burant JC, Iyengar SS, Tomasi J, Cossi M, Rega N, Millam JM, Klene M, Knox JE, Cross JB, Bakken V, Adamo C, Jaramillo J, Gomperts R, Stratmann RE, Yazyev O, Austin AJ, Cammi R, Pomelli C, Ochterski JW, Martin RL, Morokuma K, Zakrzewski VG, Voth GA, Salvador P, Dannenberg JJ, Dapprich S, Daniels AD, Farkas Ö, Foresman JB, Ortiz JV, Cioslowski J, Fox DJ (2009) Gaussian 09, Revision D.01. Gaussian Inc., Wallingford CT
47. Celani P, Werner HJ (2000) J Chem Phys 112:5546–5557
48. Celani P, Stoll H, Werner HJ, Knowles PJ (2004) Mol Phys 102:2369–2379
49. Werner HJ, Knowles PJ, Knizia G, Manby FR, Schütz M, Celani P, Korona T, Lindh R, Mitrushenkov A, Rauhut G, Shamasundar KR, Adler TB, Amos RD, Bernhardsson A, Berning A, Cooper DL, Deegan MJO, Dobbyn AJ, Eckert F, Goll E, Hampel C, Hesselmann A, Hetzer G, Hrenar T, Jansen G, Köppl C, Liu Y, Lloyd AW, Mata RA, May AJ, McNicholas SJ, Meyer W, Mura ME, Nicklass A, O'Neill DP, Palmieri P, Peng D, Pflüger K, Pitzer R, Reiher M, Shiozaki T, Stoll H, Stone AJ, Tarroni R, Thorsteinsson T, Wang M. MOLPRO, version 2012.1, a package of ab initio programs, see http://www.molpro.net
50. Blancafort L, Celani P, Bearpark MJ, Robb MA (2003) Theor Chem Acc 110:92–99
51. McWeeny R, Sutcliffe BT (1969) Molecular quantum mechanics. Academic Press, New York, pp 148–170
52. Brown CJ, Ehrenberg M (1984) Acta Crystallogr C 40:1059–1060
53. Sawada T, Mimura K, Thiemann T, Yamato T, Tashiro M, Mataka S (1998) J Chem Soc. Perkin Trans 1:1369–1371
54. Izuoka A, Murase T, Tsukada M, Ito Y, Sugawara T, Uchida A, Sato N, Inokuchi H (1997) Tetrahedron Lett 38:245–248
55. Göttle AJ, Dixon IM, Alary F, Heully JL, Boggio-Pasqua M (2011) J Am Chem Soc 133:9172–9174
56. Lebon E, Bastin S, Sutra P, Vendier L, Piau RE, Dixon IM, Boggio-Pasqua M, Alary F, Heully JL, Igau A, Juris A (2012) Chem Commun 48:741–743
57. Vieuxmaire OPJ, Piau RE, Alary F, Heully JL, Sutra P, Igau A, Boggio-Pasqua M (2013) J Phys Chem A 117:12821–12830
58. Lebon E, Sylvain R, Piau RE, Lanthony C, Pilmé J, Sutra P, Boggio-Pasqua M, Heully JL, Alary F, Juris A, Igau A (2014) Inorg Chem 53:1946–1948
59. Göttle AJ, Alary F, Dixon IM, Heully JL, Boggio-Pasqua M (2014) Inorg Chem 53:6752–6760
60. Becke AD (1993) J Chem Phys 98:5648–5652
61. Adamo C, Barone V (1999) J Chem Phys 110:6158–6170
62. Tao J, Perdew JP, Staroverov VN, Scuseria GE (2003) Phys Rev Lett 91:146401
63. Henderson TM, Izmaylov AF, Scalmani G, Scuseria GE (2009) J Chem Phys 131:044108
64. Chai JD, Head-Gordon M (2008) Phys Chem Chem Phys 10:6615–6620
65. Zhao Y, Truhlar DG (2004) J Phys Chem A 108:6908–6918
66. Yanai T, Tew DP, Handy NC (2004) Chem Phys Lett 393:51–57
67. Chai JD, Head-Gordon M (2008) J Chem Phys 128:084106
68. Becke AD (1993) J Chem Phys 98:1372–1377
69. Vydrov OA, Scuseria GE (2006) J Chem Phys 125:234109
70. Hammond GS (1955) J Am Chem Soc 77:334–338
71. Malrieu JP, Trinquier G (2012) J Phys Chem A 116:8226–8237
72. Saito T, Thiel W (2012) J Phys Chem A 116:10864–10869